

A metamaterial solid-state terahertz phase modulator

Hou-Tong Chen^{1*}, Willie J. Padilla², Michael J. Cich³, Abul K. Azad¹, Richard D. Averitt⁴ and Antoinette J. Taylor¹

Over the past two decades, terahertz time-domain spectroscopy¹ and quantum-cascade lasers² have been two of the most important developments in terahertz science and technology. These technologies may contribute to a multitude of terahertz applications that are currently under investigation globally³. However, the devices and components necessary to effectively manipulate terahertz radiation require substantial development beyond what has been accomplished to date. Here we demonstrate an electrically controlled planar hybrid metamaterial device that linearly controls the phase of terahertz radiation with constant insertion loss over a narrow frequency band. Alternatively, our device may operate as a broadband terahertz modulator because of the causal relation between the amplitude modulation and phase shifting. We perform terahertz time-domain spectroscopy, in which our hybrid metamaterial modulator replaces a commercial mechanical optical chopper, demonstrating comparable broadband performance and superior high-speed operation.

The controllable properties of engineered metamaterials facilitate novel opportunities for manipulating electromagnetic radiation⁴. Electromagnetic phenomena achieved with metamaterials include negative index of refraction^{5,6}, super-resolution in optical imaging^{7,8}, and electromagnetic invisibility⁹. The resonant electromagnetic response originates from patterned metallic subwavelength structures, in which the dimensions can be appropriately scaled to operate at terahertz frequencies^{10,11} where natural material response is somewhat rare. As such, metamaterials provide the basis for the construction of novel terahertz devices. Terahertz metamaterial devices have been demonstrated as state-of-the-art frequency-agile far-infrared filters^{12,13}, all-optical switches and modulators^{14,15}, and perfect absorbers^{16,17}. Room-temperature, voltage-controlled metamaterial devices consisting of a single unit cell layer in the propagation direction have also been shown and are of particular interest here^{18,19}.

Despite the rapid progress in terahertz technology generally, a component largely unavailable as yet is an efficient terahertz phase shifter. Its counterparts at microwave and optical frequencies have many important applications, including, for example, phased array antennas and high-speed Mach-Zehnder modulators. However these configurations are, in general, difficult to extend to the terahertz regime. There have been a few attempts to demonstrate terahertz phase shifters, including using semiconductor quantum-well structures at cryogenic temperatures^{20,21}, or liquid crystals with very low speed²². The single-layer planar hybrid metamaterial phase modulator presented in this paper overcomes these shortcomings. Although phase shifting of terahertz radiation may be inferred

from our earlier work^{13,18}, where frequency tuning of a metamaterial resonance and amplitude modulation were reported, phase modulation was not explicitly discussed or explored. Here we present the first experimental demonstration of a room-temperature solid-state phase modulator at terahertz frequencies as well as an investigation of its potential applications. Our new device achieves a voltage-controlled linear phase shift of $\sim\pi/6$ radians at 16 V. Moreover, the causal relation between amplitude switching and phase shifting enables broadband modulation.

A single unit cell of the device is illustrated schematically in Fig. 1a. Metallic electric split-ring resonators (SRRs)²³ were patterned to form a square array and connected by metal wires. They were fabricated on a 1- μm -thick epitaxial *n*-doped GaAs layer with an electron density of $2 \times 10^{16} \text{ cm}^{-3}$ grown on an intrinsic GaAs wafer. The SRRs and semiconductor form the Schottky diode structure that can, upon application of an external voltage, actively modify the depletion zone (see Supplementary Information). The control of the carrier density in the depletion zone permits tuning of the local dielectric properties near the gaps of the SRRs. This results in changes of the transmission (amplitude, phase, or both) of the metamaterial device. The micro-fabrication of the device has been described previously^{18,19}; an optical microscopy image is shown in Fig. 1b. For this design, the SRR gaps are located at the four outer corners and are directly connected to the ohmic contact through the *n*-GaAs epilayer. This maximizes depletion of electrons near the metamaterial gaps upon application of bias voltage, which is essential to control the metamaterial resonances. In an earlier metamaterial switch¹⁸, the split gap was located at the centre of an electric SRR and was surrounded by a closed outer ring. This reduced the voltage available for effective charge depletion within the split gap, which limited device performance. (See Supplementary Information for further details of the device.)

Conventional terahertz time-domain spectroscopy²⁴ (see Supplementary Information) was used to characterize the device. Resonances at 0.81 and 1.7 THz (driven by the electrical component of the terahertz radiation as indicated in Fig. 1b) are obtained as shown in Fig. 2a and b. The resonance at 0.81 THz arises from the individual SRRs and is due to the inductive-capacitive coupling of the circulating currents (Fig. 1c), while the resonance at 1.7 THz originates from a collective dipolar resonance (Fig. 1d), where the resonance frequency also depends on the SRR periodicity²⁵. At zero voltage bias the resonances are weak because carriers in the substrate shunt the metamaterial capacitive gaps, thereby damping the response. Under reverse bias voltage an increase in depletion occurs, reducing the damping and causing an increase in oscillator strength for both resonances. The depletion near the split gaps plays

¹Center for Integrated Nanotechnologies, Materials Physics & Applications Division, Los Alamos National Laboratory, Los Alamos, New Mexico 87545, USA, ²Department of Physics, Boston College, 140 Commonwealth Avenue, Chestnut Hill, Massachusetts 02467, USA, ³Sandia National Laboratories, MS1085, Albuquerque, New Mexico 87185, USA, ⁴Department of Physics, Boston University, 590 Commonwealth Avenue, Boston, Massachusetts 02215, USA; *e-mail: chenht@lanl.gov

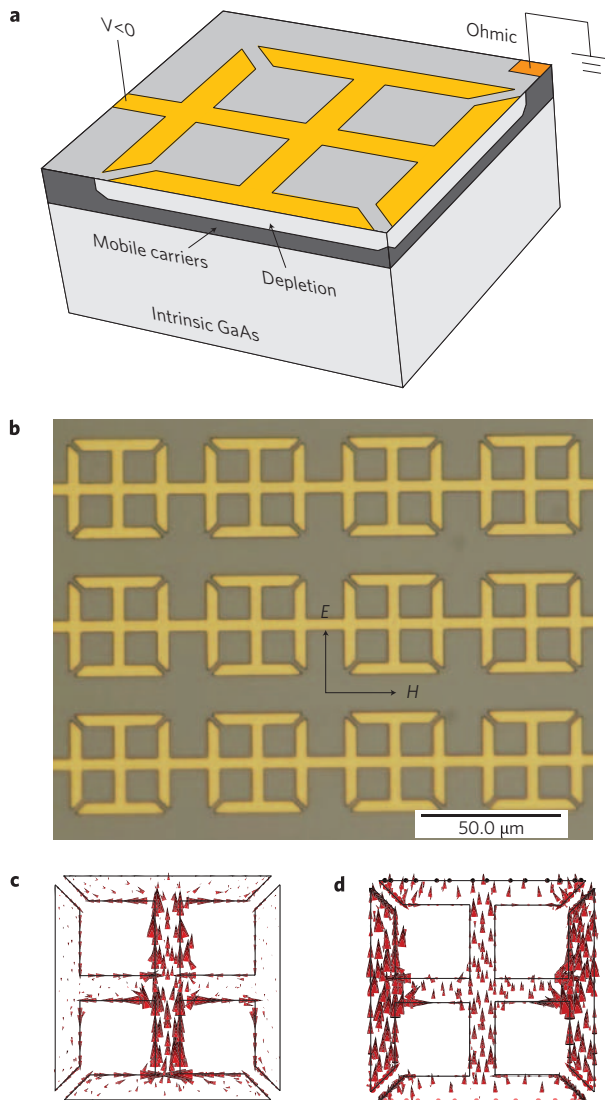


Figure 1 | Design of the electrically driven terahertz metamaterial phase shifter. **a**, Schematic of device unit cell and its cross-section, indicating the principle of operation. **b**, Optical microscopy image of the active area of the device with gold thickness 200 nm, linewidth 4 μm , split gap spacing 2 μm , outer dimension 36 μm , and period 50 μm . The polarization of the normally incident terahertz radiation is also indicated. **c,d**, Numerical simulations of surface current density excited from the inductive–capacitive (**c**) and collective dipolar (**d**) resonances at 0.81 and 1.7 THz, respectively.

a critical role in restoring resonances, as illustrated in Fig. 1c and d of the resonant surface current density.

In comparison to previously published results on metamaterial switches¹⁸, this device has a higher modulation index of the transmission amplitude. At 16 V, the amplitude of the transmitted terahertz electric field at 0.81 THz, indicated by the dashed vertical line in Fig. 2a, has decreased from $t_{0V} = 0.56$ to $t_{16V} = 0.25$, a change of 55% (intensity change of 80%), as shown in Fig. 2a. This is an 83% performance improvement over the earlier demonstration. The transmission amplitude at 1.7 THz has decreased from $t_{0V} = 0.48$ to $t_{16V} = 0.30$. Between the two resonances the reverse voltage bias significantly increases the terahertz transmission amplitude. In short, the improved device performance results from more effective depletion of charge carriers in the split gaps under an external voltage bias.

Voltage switching of the metamaterial device yields another important functionality—phase shifting of the terahertz radiation.

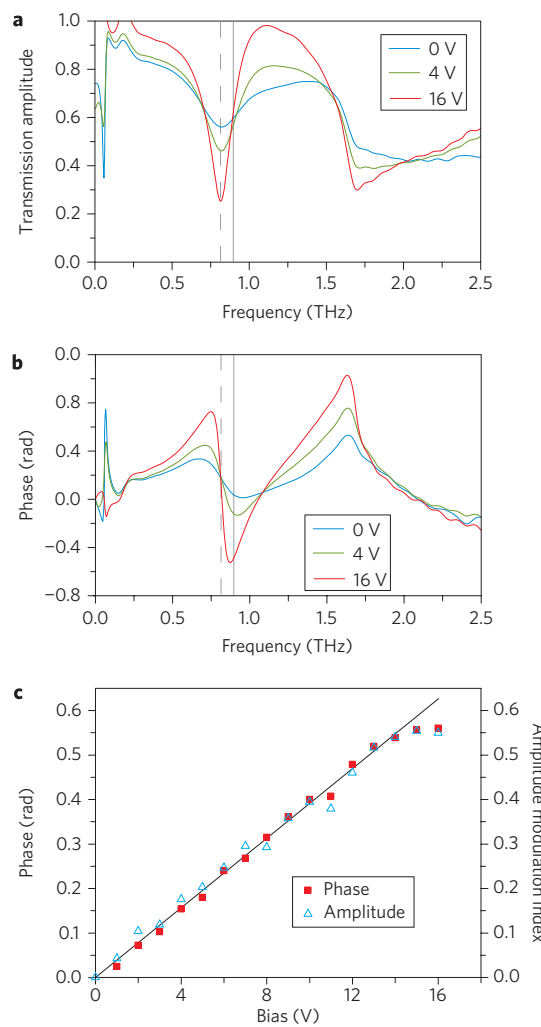


Figure 2 | Electrically controllable terahertz transmission spectra.

a,b, Transmission amplitude (**a**) and phase spectra (**b**) at 0 V and reverse bias voltages of 4 and 16 V. The solid vertical line indicates the frequencies having a large phase shift and unchanged amplitude, and the dashed vertical line indicates the frequencies having maximum amplitude switching and minimum phase shifting. **c**, Voltage dependence of the phase shift at 0.89 THz and amplitude switching (modulation depth) at 0.81 THz. The straight line is to guide the eye and indicates a linear dependence.

As shown in Fig. 2b, at 0.89 THz, indicated by the solid vertical line, the phase of terahertz transmission is $\phi_{16V} = -0.51 \text{ rad}$ under a reverse bias voltage of 16 V as compared to $\phi_{0V} = 0.05 \text{ rad}$ with no voltage bias, resulting in a shift of $\Delta\phi = 0.56 \text{ rad}$. The phase shift occurs over a bandwidth of $\sim 23 \text{ GHz}$ (that is, 0.880–0.903 THz) with a change in amplitude of less than 10% over this range. This phase change occurs within a single metamaterial unit cell in the propagation direction. A multi-layer phase shifter based on our design would enable the ultimate goal of a 2π phase shifter. Additionally, at the operational frequency of the phase shifter, the terahertz transmission amplitude is near 60% without consideration of the substrate insertion loss and is almost independent of the applied voltage bias. This is advantageous because the terahertz phase shifter can operate with reasonably high and constant terahertz transmission amplitude. The substrate insertion loss could be lowered with metamaterial impedance-matched layers²⁶.

Various interconnect schemes would permit addressing individual SRR elements, thus permitting application of, for example, a voltage

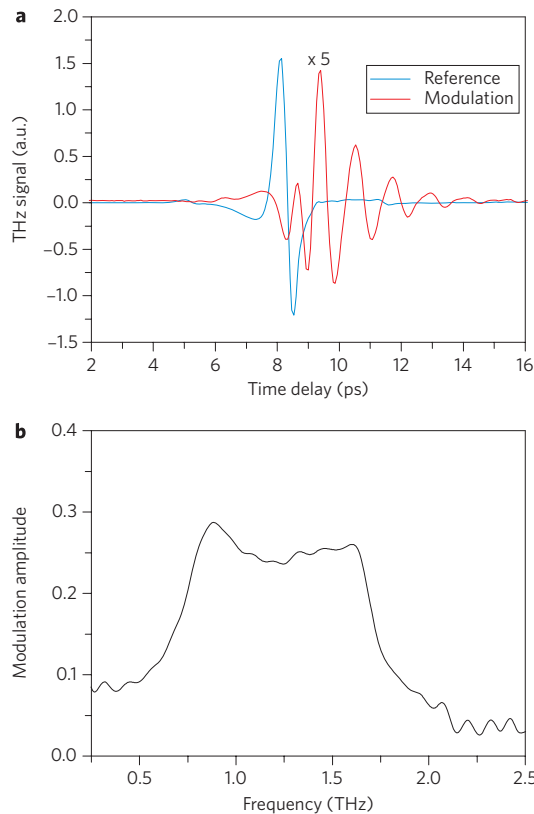


Figure 3 | Broadband modulation of terahertz radiation. **a**, Time-domain measurements of the terahertz modulation (differential) signal with a square-wave voltage bias alternating between 0 and 16 V. The reference terahertz signal is measured through a bare substrate using the terahertz time-domain system with a mechanical chopper. **b**, After Fourier transformation, the complex modulation in frequency domain is divided by the reference so that the modulation amplitude spectrum is obtained. In the frequency range roughly between the two resonances, the terahertz signal is most effectively modulated.

gradient (and associated phase shift) to the array. This would allow for real-time beam steering, focusing and other manipulations of terahertz radiation for applications such as personnel screening in airports, or locking a terahertz beam from a moving satellite to a specific receiver. Therefore, it is important to characterize the phase shift, $\Delta\phi(\omega) = |\phi_V(\omega) - \phi_{0V}(\omega)|$ as a function of the applied bias voltage. Figure 2c reveals a linear phase shift as a function of the bias voltage over the range 0–16 V at 0.89 THz. Saturation sets in at higher voltage as the resonance is restored, and because of a reduction in the Schottky resistance resulting from increased leakage currents. In Fig. 2c we also plot the voltage-dependent amplitude modulation index, $M = |t_V(\omega) - t_{0V}(\omega)|/t_{0V}(\omega)$ at 0.81 THz, which reveals a similar linear dependence. We note that the metamaterial device directly manipulates terahertz waves. This is an important distinction because alternative methods yield modulation during the terahertz generation process^{27,28}, that is, modulated sources. Thus our metamaterial device is a true ‘terahertz component’, and can be combined with various terahertz sources such as backward wave oscillators or terahertz quantum-cascade lasers.

We now turn towards a demonstration of our metamaterial device as a terahertz modulator by replacing a commercial modulator (that is, a mechanical optical chopper) in a terahertz time-domain spectroscopic system. Figure 2 indicates that amplitude switching and phase shifting in our terahertz metamaterial device are inherently narrowband—a result of the resonant nature of metamaterials. However, as shown in Fig. 2a

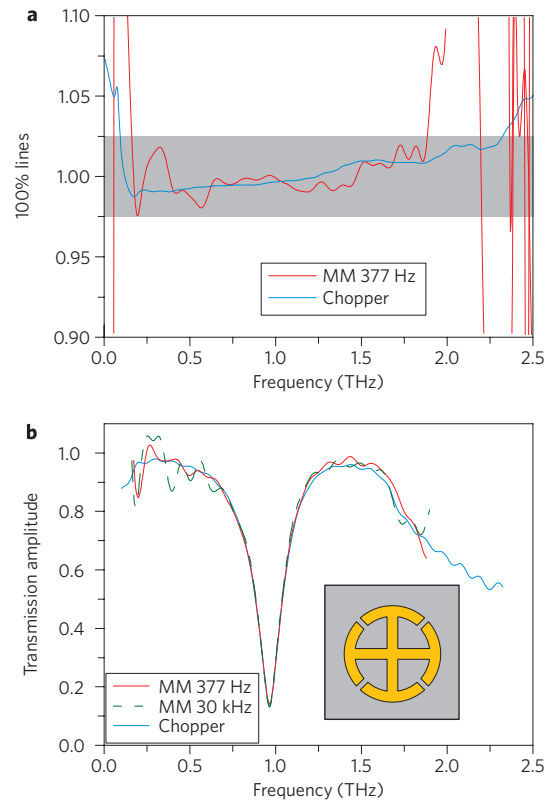


Figure 4 | Terahertz time-domain spectroscopy using the broadband metamaterial modulator. **a**, Amplitude spectral ratio of two subsequent measurements (100% lines) using the metamaterial device or a mechanical optical chopper as the modulator in a terahertz time-domain system, both at a modulation frequency of 377 Hz. The grey shaded area indicates the $\pm 2.5\%$ noise deviation. **b**, Terahertz transmission amplitude spectra through a second metamaterial sample (unit cell shown in the inset) using the metamaterial modulator (377 Hz and 30 kHz) or a mechanical optical chopper (377 Hz).

and b, the transmission amplitude and phase are not independent of each other, but are causally connected, as manifested by Kramers–Kronig (KK) relations²⁹. Specifically, the phase is proportional to the derivative of the amplitude with respect to the frequency. Near frequencies where the amplitude is not strongly dependent on the applied bias voltage, but its slope is, the phase experiences a maximum shift, and vice versa. Thus, although the amplitude modulation and phase shifting response are inherently narrowband and strongly frequency dependent, the KK relations specify that the metamaterial depicted in Fig. 1a will modulate over an extended range. Thus, our device can be used as a broadband modulator.

The frequency-dependent modulation of terahertz transmission is given by

$$|\tilde{\Delta t}(\omega)| = |t_{V1}(\omega)e^{i\phi_{V1}(\omega)} - t_{V2}(\omega)e^{i\phi_{V2}(\omega)}| \quad (1)$$

showing that the amplitude and phase contribute to the modulation. Figure 3a presents the experimental results of the metamaterial device acting as a broadband modulator. The time-domain waveform of the terahertz modulation (differential) signal is shown as the red curve for application of a square-wave voltage bias alternating between 0 and 16 V. The mechanical optical chopper has been removed from the terahertz time-domain system. As a reference, the terahertz transmission signal through a bare GaAs substrate is also measured. The modulated terahertz spectrum produced by the metamaterial device is shown in Fig. 3b and displays a broadband

and rather flat response of $\Delta t(\omega) \approx 25\%$ between 0.8 and 1.7 THz, beyond which the terahertz radiation is also modulated but with decreasing modulation depth. These frequencies correspond to the two metamaterial resonances shown in Fig. 2. By using methods to increase the frequency span between the two resonances³⁰, it is possible to further broaden the modulation bandwidth.

This terahertz modulator can be implemented into a terahertz time-domain spectrometer, replacing the typical mechanical optical chopper. To further evaluate the performance, in Fig. 4a we plot the division of two subsequent measurements, a so-called 100% line, at the modulation frequency of 377 Hz. This quantity represents the frequency-dependent noise of the system as deviations from 100%. We take as our evaluation point deviations of $\pm 2.5\%$, indicated by the grey area of Fig. 4a. The same procedure is also performed for a mechanical optical chopper at the same modulation frequency. The mechanical chopper yields a range from 93 GHz to 2.32 THz in this particular terahertz system, where the noise is mainly from the long-term system stability. The metamaterial modulator range is from 161 GHz to 1.88 THz. For a more restrictive criterion of $\pm 1\%$, the metamaterial device achieves a modulation range from 0.61 to 1.69 THz, roughly between the two resonance frequencies. The signal-to-noise ratio is not as good as the mechanical chopper, which achieves a 100% modulation depth with no insertion loss, and has, in principle, infinite bandwidth. We also note that operating this device as a broadband modulator requires phase-sensitive detection. However, the compact metamaterial modulator has no moving parts, is only 1 μm thick (one layer of active material), and has been demonstrated to operate up to 2 MHz (ref. 19), which can reduce the signal acquisition time. In contrast, mechanical optical choppers are bulky and are limited to kilohertz modulation rates.

As a further test, we performed terahertz transmission measurements through a second metamaterial sample (see inset to Fig. 4b) using our metamaterial device as a chopper (377 Hz). In Fig. 4b the transmitted amplitude spectra are shown, clearly identifying the metamaterial resonance near 1 THz. The results are comparable to those measured using a mechanical chopper (377 Hz). The agreement in Fig. 4 confirms the applicability of this metamaterial modulator as a functional device. Figure 4b also shows results at 30 kHz, significantly exceeding the operational frequency of mechanical choppers. Comparable performance to the results obtained at 377 Hz demonstrates the high-speed modulation capability.

In conclusion, we have demonstrated a single-layer, electrically controllable terahertz metamaterial phase shifter yielding up to $\Delta\phi = 0.56$ rad with constant insertion loss. The phase shifting, as well as the amplitude modulation index, reveal a linear dependence on the applied voltage bias. It is possible to individually address the metamaterial elements, which could be useful for future terahertz devices such as voltage-controlled arrays for active beam steering and focusing. This metamaterial device has been shown to modulate a complex transmission signal, and we have demonstrated its use as a high-speed broadband modulator in a terahertz time-domain spectrometer.

Received 24 November 2008; accepted 20 January 2009;
published online 22 February 2009

References

1. Grischkowsky, D., Keiding, S., van Exter, M. & Fattiger, Ch. Far-infrared time-domain spectroscopy with terahertz beams of dielectrics and semiconductors. *J. Opt. Soc. Am. B* **7**, 2006–2015 (1990).
2. Köhler, R. *et al.* Terahertz semiconductor-heterostructure lasers. *Nature* **417**, 156–159 (2002).
3. Tonouchi, M. Cutting-edge terahertz technology. *Nature Photon.* **1**, 97–105 (2007).
4. Smith, D. R., Pendry, J. B. & Wiltshire, M. C. K. Metamaterials and negative refractive index. *Science* **305**, 788–792 (2004).
5. Veselago, V. G. The electrodynamics of substances with simultaneously negative values of ϵ and μ . *Sov. Phys. Usp.* **10**, 509–514 (1968).
6. Shelby, R. A., Smith, D. R. & Schultz, S. Experimental verification of a negative index of refraction. *Science* **292**, 77–79 (2001).
7. Pendry, J. B. Negative refraction makes a perfect lens. *Phys. Rev. Lett.* **85**, 3966–3969 (2000).
8. Fang, N., Lee, H., Sun, C. & Zhang, X. Sub-diffraction-limited optical imaging with a silver superlens. *Science* **308**, 534–537 (2005).
9. Schurig, D. *et al.* Metamaterial electromagnetic cloak at microwave frequencies. *Science* **314**, 977–980 (2006).
10. Yen, T. J. *et al.* Terahertz magnetic response from artificial materials. *Science* **303**, 1494–1496 (2004).
11. Azad, A. K., Dai, J. & Zhang, W. Transmission properties of terahertz pulses through subwavelength double split-ring resonators. *Opt. Lett.* **31**, 634–636 (2006).
12. Chen, H.-T. *et al.* Complementary planar terahertz metamaterials. *Opt. Express* **15**, 1084–1095 (2007).
13. Chen, H.-T. *et al.* Experimental demonstration of frequency-agile terahertz metamaterials. *Nature Photon.* **2**, 295–298 (2008).
14. Padilla, W. J., Taylor, A. J., Highstrete, C., Lee, M. & Averitt, R. D. Dynamical electric and magnetic metamaterial response at terahertz frequencies. *Phys. Rev. Lett.* **96**, 107401 (2006).
15. Chen, H.-T. *et al.* Ultrafast optical switching of terahertz metamaterials fabricated on ErAs/GaAs nanoisland superlattices. *Opt. Lett.* **32**, 1620–1622 (2007).
16. Landy, N. I., Sajuyigbe, S., Mock, J. J., Smith, D. R. & Padilla, W. J. Perfect metamaterial absorber. *Phys. Rev. Lett.* **100**, 207402 (2008).
17. Tao, H. *et al.* A metamaterial absorber for the terahertz regime: Design, fabrication and characterization. *Opt. Express* **16**, 7181–7188 (2008).
18. Chen, H.-T. *et al.* Active terahertz metamaterial devices. *Nature* **444**, 597–600 (2006).
19. Chen, H.-T. *et al.* Hybrid metamaterials enable fast electrical modulation of freely propagating terahertz waves. *Appl. Phys. Lett.* **93**, 091117 (2008).
20. Libon, I. H. *et al.* An optically controllable terahertz filter. *Appl. Phys. Lett.* **76**, 2821–2823 (2000).
21. Kersting, R., Strasser, G. & Unterrainer, K. Terahertz phase modulator. *Electron. Lett.* **36**, 1156–1158 (2000).
22. Hsieh, C.-F., Pan, R.-P., Tang, T.-T., Chen, H.-L. & Pan, C.-L. Voltage-controlled liquid-crystal terahertz phase shifter and quarter-wave plate. *Opt. Lett.* **31**, 1112–1114 (2006).
23. Padilla, W. J. *et al.* Electrically resonant terahertz metamaterials: Theoretical and experimental investigations. *Phys. Rev. B* **75**, 041102(R) (2007).
24. O'Hara, J. F., Zide, J. M. O., Gossard, A. C., Taylor, A. J. & Averitt, R. D. Enhanced terahertz detection via ErAs:GaAs nanoisland superlattices, *Appl. Phys. Lett.* **88**, 251119 (2006).
25. Acuna, G. *et al.* Surface plasmons in terahertz metamaterials. *Opt. Express* **16**, 18745–18751 (2008).
26. Lee, J. W. *et al.* Invisible plasmonic meta-materials through impedance matching to vacuum. *Opt. Express* **13**, 10681–10687 (2005).
27. Zhao, G., Schouten, R. N., van der Valk, N., Wenckebach, W. Th. & Planken, P. C. M. Design and performance of a THz emission and detection setup based on a semi-insulating GaAs emitter. *Rev. Sci. Instrum.* **73**, 1715–1719 (2002).
28. Cai, Y. *et al.* Coherent terahertz radiation detection: Direct comparison between free-space electro-optic sampling and antenna detection. *Appl. Phys. Lett.* **73**, 444–446 (1998).
29. Jackson, J. D. *Classical Electrodynamics* 3rd edn (John Wiley & Sons, 1998).
30. Azad, A. K., Taylor, A. J., Smirnova, E. & O'Hara, J. F. Characterization and analysis of terahertz metamaterials based on rectangular split-ring resonators. *Appl. Phys. Lett.* **92**, 011119 (2008).

Acknowledgements

We thank I. Brener for coordinating the sample fabrication, J.F. O'Hara for discussions and the use of the terahertz system, and D. Lippens for useful discussions. We acknowledge support from the Los Alamos National Laboratory LDRD Program. This work was performed, in part, at the Center for Integrated Nanotechnologies, a US Department of Energy, Office of Basic Energy Sciences Nanoscale Science Research Center operated jointly by Los Alamos and Sandia National Laboratories. Los Alamos National Laboratory, an affirmative action/equal opportunity employer, is operated by Los Alamos National Security, LLC, for the National Nuclear Security Administration of the US Department of Energy under contract DE-AC52-06NA25396.

Additional information

Supplementary Information accompanies this paper at www.nature.com/naturephotronics. Reprints and permission information is available online at <http://npg.nature.com/reprintsandpermissions/>. Correspondence and requests for materials should be addressed to H.T.C.